

---

---

# Development of $^{124}\text{I}$ Immuno-PET Targeting Tumor Vascular TEM1/Endosialin

Ann-Marie Chacko\*<sup>1,2</sup>, Chunsheng Li\*<sup>3</sup>, Madhura Nayak<sup>1</sup>, John L. Mikitsh<sup>1</sup>, Jia Hu<sup>3</sup>, Catherine Hou<sup>1</sup>, Luigi Grasso<sup>4</sup>, Nicholas C. Nicolaidis<sup>4</sup>, Vladimir R. Muzykantov<sup>2</sup>, Chaitanya R. Divgi<sup>1</sup>, and George Coukos<sup>3</sup>

<sup>1</sup>Division of Nuclear Medicine and Clinical Molecular Imaging, Department of Radiology, Perelman School of Medicine, University of Pennsylvania, Philadelphia, Pennsylvania; <sup>2</sup>Institute for Translational Medicine and Therapeutics, Perelman School of Medicine, University of Pennsylvania, Philadelphia, Pennsylvania; <sup>3</sup>Ovarian Cancer Research Center, Perelman School of Medicine, University of Pennsylvania, Philadelphia, Pennsylvania; and <sup>4</sup>Morphotek, Inc., Exton, Pennsylvania

Tumor endothelial marker 1 (TEM1/endosialin) is a tumor vascular marker highly overexpressed in multiple human cancers with minimal expression in normal adult tissue. In this study, we report the preparation and evaluation of  $^{124}\text{I}$ -MORAb-004, a humanized monoclonal antibody targeting an extracellular epitope of human TEM1 (hTEM1), for its ability to specifically and sensitively detect vascular cells expressing hTEM1 in vivo. **Methods:** MORAb-004 was directly iodinated with  $^{125}\text{I}$  and  $^{124}\text{I}$ , and in vitro binding and internalization parameters were characterized. The in vivo behavior of radioiodinated MORAb-004 was characterized in mice bearing subcutaneous ID8 tumors enriched with mouse endothelial cells expressing hTEM1 and by biodistribution and small-animal immuno-PET studies. **Results:** MORAb-004 was radiolabeled with high efficiency and isolated in high purity. In vitro studies demonstrated specific and sensitive binding of MORAb-004 to MS1 mouse endothelial cells expressing hTEM1, with no binding to control MS1 cells.  $^{125}\text{I}$ -MORAb-004 and  $^{124}\text{I}$ -MORAb-004 both had an immunoreactivity of approximately 90%. In vivo biodistribution experiments revealed rapid, highly specific and sensitive uptake of MORAb-004 in MS1-TEM1 tumors at 4 h ( $153.2 \pm 22.2$  percentage injected dose per gram [%ID/g]), 24 h ( $127.1 \pm 42.9$  %ID/g), 48 h ( $130.3 \pm 32.4$  %ID/g), 72 h ( $160.9 \pm 32.1$  %ID/g), and 6 d ( $10.7 \pm 1.8$  %ID/g). Excellent image contrast was observed with  $^{124}\text{I}$ -immuno-PET. MORAb-004 uptake was statistically higher in TEM1-positive tumors than in control tumors. Binding specificity was confirmed by blocking studies using excess nonlabeled MORAb-004. **Conclusion:** In our preclinical model, with hTEM1 exclusively expressed on engineered murine endothelial cells that integrate into the tumor vasculature,  $^{124}\text{I}$ -MORAb-004 displays high tumor-to-background tissue contrast for detection of hTEM1 in easily accessible tumor vascular compartments. These studies strongly suggest the clinical utility of  $^{124}\text{I}$ -MORAb-004 immuno-PET in assessing TEM1 tumor-status.

**Key Words:** immuno-PET; TEM1; endosialin; MORAb-004; monoclonal antibodies

**J Nucl Med 2014; 55:500–507**

DOI: 10.2967/jnumed.113.121905

---

Received Mar. 7, 2013; revision accepted Nov. 11, 2013.

For correspondence contact: Ann-Marie Chacko, 231 S. 34th St., Rm. 288, Chemistry Building, Division of Nuclear Medicine and Clinical Molecular Imaging, Department of Radiology, Perelman School of Medicine, University of Pennsylvania, Philadelphia, PA 19104.

E-mail: achacko@upenn.edu

\*Contributed equally to this work.

Published online Feb. 13, 2014.

COPYRIGHT © 2014 by the Society of Nuclear Medicine and Molecular Imaging, Inc.

**T**umor vascular markers (TVMs) are attractive targets for antibody-based diagnostics and therapeutics. Targeting tumor vasculature rather than tumor cells themselves has several advantages. Among these, tumor vasculature expresses unique molecular targets that are absent in normal vasculature, vascular targets are less likely to be lost due to adaptation or mutations, and TVMs are readily accessible to blood circulation. Consequently, TVMs are attractive targets for antibody-based cancer diagnosis of molecular phenotype and personalized therapy (1–3).

Tumor endothelial marker 1 (TEM1)/endosialin/CD248 is emerging as a robust TVM in multiple human cancers (4,5). These early studies concluded that TEM1-positive cells are tumor endothelial cells. However, nearly all carcinomas, including ovarian, lung, and breast cancer, have TEM1 expression that is restricted to tumor-associated perivascular cells (pericytes) and stromal cells (6–12). In sarcomas, ranging from neuroblastoma to colorectal cancers to highly invasive glioblastomas, TEM1 is also expressed in malignant cancer cells (6,13–15). TEM1 is a heavily *O*-glycosylated 175-kDa type I transmembrane protein of the C-type lectin-like receptor family, which shares overall architecture with thrombomodulin (11). The extracellular domain contains a C-type lectin-like domain, 3 epidermal growth factor–like repeats, and a proline-rich mucin domain, whereas the intracellular domain is fairly short (51 amino acids), with 3 potential phosphorylation sites and a C-terminal PDZ-binding motif (16). This surface protein is not shed, but little is known on its modulation or internalization in response to epitope engagement by antibodies and other TEM1-targeted therapies. Its high expression on the tumor vasculature across a wide variety of solid human cancers, with limited expression in normal adult tissue, makes human TEM1 (hTEM1) an ideal target for exogenous antibody therapies and diagnostics (17–19).

A humanized IgG monoclonal antibody (mAb) directed to human endosialin/TEM1 (MORAb-004; Morphotek, Inc.) (20) is currently being explored in phase I/II clinical trials for its potential antiangiogenic and antineoplastic activity in solid and soft-tissue tumors. The efficacy of this anti-TEM1 mAb against solid tumors is also being investigated in combination with chemotherapy (21). The mechanism of action of MORAb-004 in vivo appears to be mediated by inhibiting the cell surface association of TEM1 with extracellular matrix proteins including fibronectin, collagen I/IV (20), and the Mac-2 BP/90K protein (22).

A critical factor in targeted therapy is evaluating the presence and amount of the specific target in the tumor and its relevance to the disease state. The overexpression of TEM1 on tumor vasculature

provides a potential target for the specific diagnosis and therapy of TEM1-positive (TEM1+) tumors. Initial clinical experience by immunohistochemistry analysis reveals that high TEM1 levels correlate with high tumor grade and aggressive tumor behavior (7,23). Along with other pathologic procedures and tests, noninvasive nuclear imaging is often used to assess the status of the specific target. Multiple antibodies against TEM1 have been reported (17,24), however, there is limited demonstration of whether this TVM can function as a target for tumor detection in diagnostic nuclear medicine. Considering the superiority of PET over single-photon scintigraphy, the development of an hTEM1-specific PET radioimmunoconjugate is a worthwhile pursuit. Because of its high resolution, sensitivity, and unique ability to measure tissue concentrations of radioactivity in 3 dimensions, PET is the method of choice for in vivo imaging using therapeutic and diagnostic antibodies.  $^{124}\text{I}$  is a positron-emitting radioisotope that can be attached to antibodies generally without significant loss of immunobiologic characteristics; its 4.2-d half-life allows assessment of long-term pharmacokinetics of antibody forms (25–27). To the best of our knowledge, this report represents the first study of a positron-emitting form of a TEM1-directed antibody construct in a murine mouse model of hTEM1-expressing tumor vasculature.

## MATERIALS AND METHODS

### Antibodies and Cell Lines

Humanized anti-hTEM1 MORAb-004 mAb (IgG<sub>1</sub>, 160 kDa), which binds human but not murine TEM1, was produced by Morphotek, Inc. The MS1 mouse endothelial cell line, engineered to express DsRed and firefly luciferase fLuc (for ease, designated as MS1), was used for subsequent generation of the MS1-TEM1 cell line, expressing hTEM1, and EmGFP, in addition to DsRed and fLuc (18). MS1-TEM1 cells were sorted by flow-assisted flow cytometry sorting using a MoFlo cell sorter (Dako Cytomation), and the cell population with lower hTEM1 expression was expanded and used for subsequent studies. ID8 is a mouse ovarian surface epithelium cancer cell line, provided by Dr. Paul Terranova (University of Kansas Medical Center) (28). MS1 cell lines and the ID8 cell line were maintained in RPMI 1640 containing 10% fetal bovine serum and antibiotics. Full details of all methods and equipment used are presented in the supplemental materials (available at <http://jnm.snmjournals.org>).

### Radiolabeling

Iodination of MORAb-004 mAb and control IgG<sub>1</sub> was performed by the IODO-GEN method (Pierce) (29). Briefly,  $^{125}\text{I}$ -NaI (in 0.01N NaOH; Perkin Elmer) or  $^{124}\text{I}$ -NaI (in 0.02 M NaOH; IBA Molecular) was added to a precoated iodination tube (Thermo Scientific) containing antibody (15  $\mu\text{g}$ , 1 mg/mL in phosphate-buffered saline) and incubated for 5 min. Radiolabeled antibody was purified using a 2-mL desalting column (Thermo Scientific). Trichloroacetic acid precipitation assay (30) and radio-thin-layer chromatography were used to determine radiolabeling efficiency and purity for labeled antibodies. Protein concentration was measured using Nanodrop 2000c (Thermo Scientific) to calculate specific activity (MBq/mg).

### In Vitro Characterization

**Radioimmunoassay.** Assessment of specific binding of  $^{125/124}\text{I}$ -MORAb-004 was determined by radioimmunoassay using cells grown to confluence on 1% gelatin-coated 96-strip well microplates (Corning Life Sciences). For direct mAb binding assay, cells were incubated with increasing concentration of  $^{125/124}\text{I}$ -MORAb-004 in assay buffer (5% fetal bovine serum in RPMI 1040) in quadruplicate at 4°C for 4 h. Cells were washed 5 times with ice-cold wash buffer (3% bovine serum albumin/phosphate-buffered saline). Cell-associated radioactivity was

measured by a  $\gamma$  counter (2470 Wizard<sup>2</sup>, Perkin Elmer) and normalized to the total number of cells, counted by hemocytometer. Nonspecific binding was determined using control MS1 cells or by performing the assay in 100-fold excess of unlabeled ligand. Radioimmunoassay analysis was performed as previously described (30). The details to determine the apparent binding affinity,  $K_d$ ; the number of functional binding sites per cell,  $B_{\text{max}}$ ; and the binding inhibition constant,  $K_i$ , can be found in the supplemental materials. In competitive binding assays, cells were incubated with a fixed concentration of  $^{125/124}\text{I}$ -mAb for 4 h at 4°C, in the presence of unlabeled MORAb-004 (0–200 nM). Binding data were collected as above and the competitive binding data plotted as described in the supplemental materials.

**Internalization Assay.** For fluorescent ligand assay, cells were cultured on chamber slides (Nunc; Life Technologies) overnight at 37°C in culture medium. Cells were incubated with DyLight405-MORAb-004 immunoconjugate (1 mL, 1.5 mg/mL in medium) at 4°C and allowed to warm to 37°C for 1 h. After two 5-min washes with wash buffer (or additional glycine buffer wash [pH 2; 200 mM glycine; 150 mM NaCl]), cells were fixed with 2% paraformaldehyde. Images were taken with an inverted LSM510 confocal microscope (Carl Zeiss), using a 405-nm diode laser, 488-nm argon laser, and 561-nm diode laser for excitation of Dylight405, EmGFP, and DsRed, respectively.

For the radioligand assay, cells were grown to confluence on 1% gelatin-coated 96-strip well microplates and incubated with  $^{125}\text{I}$ -MORAb-004 at 37°C at selected time points up to 24 h. Cells were placed on ice and rinsed with wash buffer. Parallel plates were washed with glycine buffer (pH 2) twice for 5 min to remove surface-bound radioactivity. Wells were counted in a  $\gamma$  counter and normalized to total activity bound.

### In Vivo Characterization

**Chimeric hTEM1-Expressing Murine Vascular Graft Model.** All animal experiments were conducted in compliance with the guidelines of the Institutional Animal Care and Use Committee. Chimeric tumors expressing hTEM1 in the vasculature were established by subcutaneous injection of  $2 \times 10^6$  ID8 cancer cells comixed with MS1-TEM1 or MS1 endothelial cells (at a ratio of 1:5 ID8 to MS1) in each mouse flank of female athymic *nu/nu* mice (CrI:NU-Foxn1<sup>tmu</sup>; weight, 18 g; age, 4–6 wk; Charles River Laboratories, Inc.). Mice were provided with food and water ad libitum. Mice with tumor grafts expressing fLuc reporter were anesthetized using 1%–2% isoflurane/O<sub>2</sub> (VetEquip), and in vivo bioluminescence imaging was performed thrice weekly using the Xenogen IVIS Lumina II small-animal imaging system (Caliper Life Science). Briefly, D-Luciferin (phosphate-buffered saline stock [150 mg/mL]; 150  $\mu\text{L}$ /15-g mouse) was injected intraperitoneally, and optical images were acquired at 10 min after injection. Pseudocolor images of emitted photon radiance (p/s/cm<sup>2</sup>/sr) were generated and quantified with Living Image Version 3.0 software (Caliper Life Science). Tumors were allowed to grow to a size of 5–10 mm in diameter (14–21 d), and then mice were used for subsequent studies.

**Biodistribution and Autoradiography Studies.** Naïve mice and mice bearing ID8 tumors comixed with MS1 or MS1-TEM1 endothelial cells were administered  $^{125}\text{I}$ -MORAb-004 (0.185 MBq [5  $\mu\text{Ci}$ ], 2.5  $\mu\text{g}$  mAb, in 150  $\mu\text{L}$  of sterile 0.9% saline for injection) via the tail vein. Animals ( $n = 3$ –6, per group) were euthanized at 4, 24, 48, 72, and 144 h after injection, and organs and tumors were removed, weighed, and counted in a  $\gamma$  counter for accumulation of activity. In a separate cohort, tumors were harvested, embedded in Tissue-TEK OCT compound (Sakura, Finetek U.S.A Inc.), and frozen at  $-80^\circ\text{C}$ . Serial 10- $\mu\text{m}$ -thick sections were cut at  $-20^\circ\text{C}$  in a cryostat (Leica CM1950). Sections were exposed to a phosphorimage plate (BAS; Fujifilm) for 48 h. Digital autoradiography images were read using a phosphor plate reader (Typhoon FLA-7000; GE Healthcare).

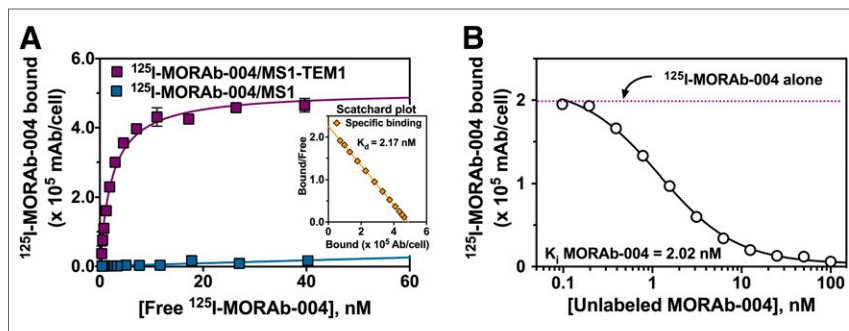


**FIGURE 1.** Cell surface binding parameters of  $^{125}\text{I}$ -MORAb-004 to MS1-TEM1 and MS1 cells by live-cell radioimmunoassay. (A) Saturation binding curve for  $^{125}\text{I}$ -MORAb-004 from representative experiment at  $4^\circ\text{C}$  for 4 h (inset shows Scatchard plot). (B) Competitive binding of  $^{125}\text{I}$ -MORAb-004 (5.0 nM) with increasing concentrations of unlabeled MORAb-004. Binding data were plotted as  $^{125}\text{I}$ -MORAb-004 bound per cell (mAb/cell).

**Immuno-PET Studies.** PET experiments were conducted on a small-animal A-PET scanner (Mosaic; Philips) with an imaging field of view of 11.5 cm (31). Mice were administered  $^{124}\text{I}$ -MORAb-004 (5.2 MBq [ $\sim 140 \mu\text{Ci}$ ], 2.5  $\mu\text{g}$  mAb, in 150  $\mu\text{L}$  of sterile 0.9% saline for injection) via tail vein injection. For blocking studies, mice were coinjected with 25  $\mu\text{g}$  of nonlabeled MORAb-004. Mice were anesthetized by inhalation of a 1%–2% isoflurane/ $\text{O}_2$  and placed on the scanner bed before the imaging study. PET data acquisition commenced at 4, 24, 48, and 72 h after injection of the radiotracer, and dynamic scans were obtained over a period of 1 h (5 min per frame; image voxel size, 0.5  $\text{mm}^3$ ). Analysis on reconstructed images was performed using AMIDE (<http://amide.sourceforge.net>). After termination of the final PET scan, mice were euthanized and tissue activity assessed.

#### Data Analysis and Statistics

All experiments were performed at least in triplicate, with a minimum of 3 independent experiments. Results are expressed as mean  $\pm$  SD unless otherwise noted. Significant differences between means were determined using 1-way ANOVA followed by a post hoc Bonferroni multiple comparison test or unpaired Student *t* test, as appropriate. Differences at the 95% confidence level ( $P < 0.05$ ) were considered statistically significant. All curve-fitting and statistical analyses were conducted using Prism 5.0 software (GraphPad).

## RESULTS

#### Radioiodination

MORAb-004 was successfully radiolabeled with near-quantitative labeling efficiency. Radiochemical purity by radio-thin-layer chromatography and trichloroacetic acid precipitation assays showed that more than 98% of  $^{125}\text{I}/^{124}\text{I}$  was bound to protein after size-exclusion column purification (Supplemental Fig. 1). Specific activities for  $^{125}\text{I}$ -MORAb-004 ranged from 150 to 225 MBq/mg

(4–6 mCi/mg; mean, 185 MBq/mg [5 mCi/mg]) and from 280 to 340 MBq/mg (7.6–9.2 mCi/mg) for IgG<sub>1</sub> control (mean, 300 MBq/mg [8.1 mCi/mg]). For  $^{124}\text{I}$ -MORAb-004, specific activities were between 1,920 and 2,220 MBq/mg (52–60 mCi/mg; mean, 2,072 MBq/mg [56 mCi/mg]).

#### In Vitro Binding Properties of MORAb-004

The specificity of binding of  $^{125}\text{I}$ -MORAb-004 to hTEM1 was assessed with mouse endothelial MS1 cells engineered and subsequently sorted to express surface TEM1 as compared with control MS1 cells. The apparent dissociation constant ( $K_d$ ) of  $^{125}\text{I}$ -MORAb-004 determined by live-cell radioimmunoassay was  $3.41 \pm 1.20$  nM, and

the number of MORAb-004 mAb bound per cell ( $B_{\text{max}}$ ) was  $6.28 \pm 2.14 \times 10^5$  (Fig. 1A).  $^{125}\text{I}$ -MORAb-004 did not bind to control MS1 cells, and binding on MS1-TEM1 cells could be blocked with excess unlabeled mAb, demonstrating specificity. Competitive binding assays demonstrated that  $^{125}\text{I}$ -MORAb-004 was displaced with increasing amounts of unlabeled MORAb-004, with the  $K_i$  of unlabeled MORAb-004 being  $3.10 \pm 1.24$  nM (Fig. 1B). mAb immunoreactivity from radioimmunoassay was approximately 90% for both  $^{125}\text{I}$ -MORAb-004 and  $^{124}\text{I}$ -MORAb-004 after direct iodination at the noted specific activity (Table 1).  $^{125}\text{I}$ -MORAb-004 bound to endogenous hTEM1 with higher affinity ( $K_d \sim 0.5$  nM) when incubated with human neuroblastoma LA1-5s cells, as compared with recombinant hTEM1 expressed in the murine MS1-TEM1 cell line (Supplemental Fig. 2). The number of surface hTEM1 molecules is comparable between LA1-5s cells and MS1-TEM1 cells.

#### Internalization of MORAb-004

To qualitatively assess mAb internalization after binding to TEM1, we followed the location of fluorescent dye-labeled MORAb-004 (MORAb-004-Dy405) on MS1-TEM1 cells versus control MS1 cells by confocal microscopy. Cells were initially incubated with MORAb-004-Dy405 on ice and then allowed to warm to  $37^\circ\text{C}$ . At  $4^\circ\text{C}$ , MORAb-004-Dy405 (blue) localized to the cell membrane on MS1-TEM1 cells (Fig. 2A), but there was no binding on MS1 cells (Fig. 2E). Surface binding could be effectively removed after acid wash, showing that signal was restricted to the plasma membrane at  $4^\circ\text{C}$  (Fig. 2B). After warming to  $37^\circ\text{C}$  for 1 h, strong immunofluorescence was observed on both plasma membrane and in intracellular compartments of MS1-TEM1 cells (Fig. 2C). Internalization of MORAb-004-Dy405 was confirmed by acid wash of MS1-TEM1 cells, where surface-bound mAb was

**TABLE 1**  
Binding Parameters of antiTEM1 IgG<sub>1</sub> MORAb-004 mAb to Live MS1 Cells Expressing hTEM1\*

mAb	Specific activity (MBq/mg)	$K_d$ (nM)	$B_{\text{max}}$ ( $\times 10^5$ mAb/cell)	Immunoreactivity <sup>†</sup>
$^{125}\text{I}$ -MORAb-004 ( $n = 5$ )	150–225	$3.41 \pm 1.20$	$6.28 \pm 2.14$	$90.1\% \pm 4.8\%$
$^{124}\text{I}$ -MORAb-004 ( $n = 3$ )	1920–2220	$3.41 \pm 0.93$	$7.52 \pm 1.92$	$90.1\% \pm 1.5\%$

\*MS1 cells used as binding control; results expressed as mean  $\pm$  SD.

<sup>†</sup>Immunoreactivity =  $K_d$   $^{125}\text{I}/^{124}\text{I}$ -MORAb-004/ $K_i$  unlabeled MORAb-004.

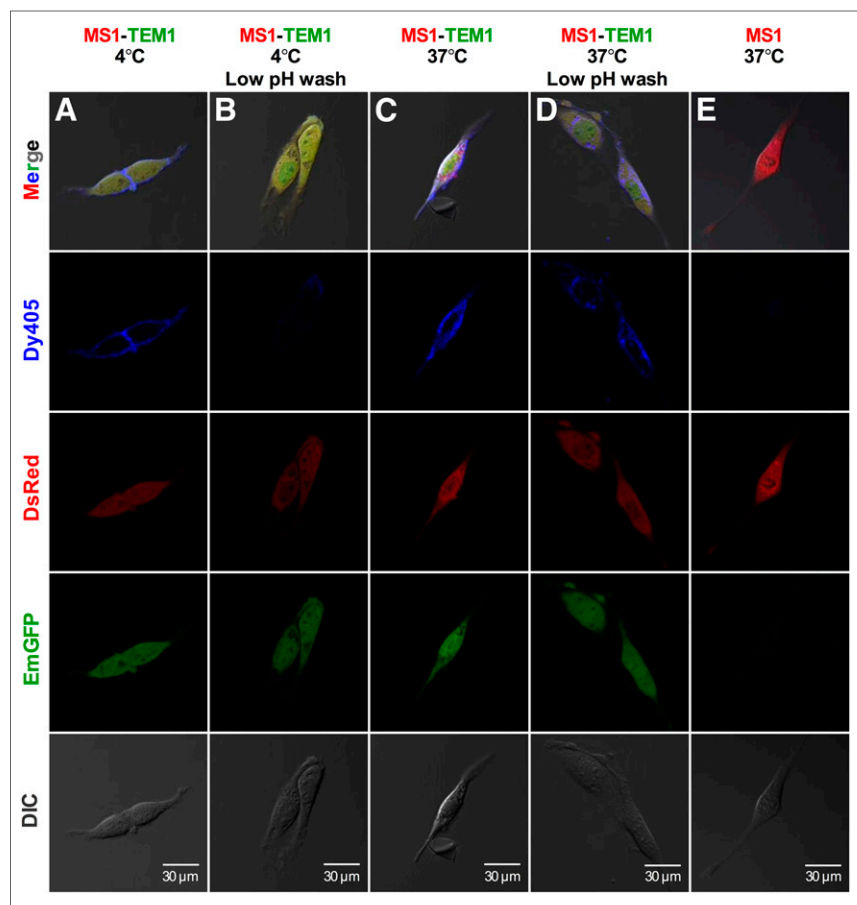


**FIGURE 2.** Confocal immunofluorescence microscopy of MS1-TEM1 (A–D) and MS1 (E) cells incubated with fluorescent immunoconjugate MORAb-004-DyLight405 (Dy405; blue) shows that MORAb-004 is internalized in MS1-TEM1 cells. MS1-TEM1 cells were transfected with DsRed (red) and GFP (green), whereas MS1 cells express only DsRed (Red). MORAb-004-Dy405 localized to cell surface membrane of MS1-TEM1 cells at 4°C for 1 h (A) and could be effectively removed after low pH wash (B). After 1 h at 37°C, MORAb-004 was observed on cell surface and in intracellular compartments of MS1-TEM1 cells (C), with intracellular fraction still evident after low pH wash (D). MORAb-004 did not bind to MS1 cells (E). Merging of blue, red, and green channel with differential interference contrast (DIC) image is shown in topmost box in A–E. Scale bar in DIC panel is 30  $\mu\text{m}$ .

removed but intracellular MORAb-004-Dy405 was still retained (Fig. 2D).

For quantitative assessment of MORAb-004 internalization, MS1-TEM1 cells were incubated with  $^{125}\text{I}$ -MORAb-004 and the internalization of MORAb-004 was studied by  $\gamma$  counting (Fig. 3). The fraction of radioactivity that internalized in MS1-TEM1 cells at 2 h at 37°C was approximately 12% of total activity bound and did not change with increasing dose of  $^{125}\text{I}$ -mAb added to the medium (0.5–4 nM) (Fig. 3A). The fraction of radioactivity that internalized in MS1-TEM1 cells, with respect to the total amount of  $^{125}\text{I}$ -MORAb-004 bound per MS1-TEM1 cell, increased from 15.6%  $\pm$  0.7% at 2 h to 23.4%  $\pm$  0.9% at 4 h and reached a plateau at 8 h from 32.8%  $\pm$  0.8% to 38.6%  $\pm$  0.9% at 24 h (Figs. 3B and 3C). Interestingly, in LA1-5s neuroblastoma cells, which endogenously express hTEM1, maximum internalization was achieved at 60 min and remained quite low at less than 10% at all time points thereafter (Supplemental Fig. 3). The uptake of radioactivity was completely blocked by the addition of unlabeled MORAb-004 to the incubation medium, thus demonstrating the requirement of TEM1-specific binding

in mediating internalization. Figures 3B and 3C show the internalized and surface-bound fractions over time, with respect to total cell bound radioactivity. The surface-bound fraction of radioactivity was the activity removed from the total bound activity after an acid wash of the cells.

### In Vivo Characterization

**Biodistribution Studies.** In naïve non-tumor-bearing mice, there was a dramatic difference in the blood clearance kinetics of  $^{125}\text{I}$ -MORAb-004, as compared with mice bearing ID8 tumor grafts enriched with MS1 or MS1-TEM1 endothelial cells in either flank (Fig. 4; Tables 2 and 3). In naïve mice, the blood-pool activity was 22.39  $\pm$  1.47 percentage injected dose per gram (%ID/g) at 4 h and slowly decreased 4-fold to 5.64  $\pm$  0.50 %ID/g on day 6. Blood-pool activity decreased 25-fold over a 6-d period, from 18.84  $\pm$  0.93 %ID/g at 4 h to 0.74  $\pm$  0.05 %ID/g on day 6. There was slower washout of activity across all major organs, as seen with blood levels, in naïve mice, as compared with tumor-bearing mice. In contrast, uptake in TEM1+ tumor grafts was 153.19  $\pm$  22.24 %ID/g as early as 4 h after injection and remained consistently high out to 3 d after injection, demonstrating retention of the TEM1-targeted antibody. Uptake in TEM1+ tumors decreased to 10.65  $\pm$  1.08 %ID/g at 6 d after injection. Uptake in TEM1-negative (TEM1–) tumor grafts was significantly lower than TEM1+ tumors at all time points, with uptake clearing over time from 8.98  $\pm$  2.48 %ID/g at 4 h to 3.93  $\pm$  1.98 %ID/g at 72 h and 0.67  $\pm$  0.08 %ID/g on day 6. Autoradiography of tumors at 24 h after injection further confirmed the higher uptake of  $^{125}\text{I}$ -MORAb-004 in TEM1+ tumors than in the control tumors

(Fig. 4C). The tumor-to-blood ratio in TEM1+ grafts increased 4.5-fold from 8.1 to a maximum of 40.6 on day 3. Similarly, the TEM1+ to-TEM1– tumor ratio in ID8 grafts increased 2.7-fold from 18.1 to a maximum of 49.1 on day 3. Target-to-nontarget uptake ratios were decreased by day 6. As an indication of radioiodine metabolism from the antibody, thyroid uptake was also assessed over time. No time-dependent changes in thyroid uptake were observed in both naïve and tumor-bearing mice up to 6 d after injection. Thyroid levels ranged from 0.1% to 1.2 %ID per total organ (%ID/org).

The specificity of TEM1 tumor targeting was demonstrated using an isotype control IgG<sub>1</sub>. The biodistribution of  $^{125}\text{I}$ -IgG<sub>1</sub> shows that uptake of the nontargeted IgG is nearly the same between both MS1-TEM1 and MS1 vascularized tumors, with 5.43  $\pm$  0.73 and 5.13  $\pm$  1.86 %ID/g at 24 h after injection, respectively (supplemental materials). The localization ratio of TEM1+ tumor uptake to blood and TEM1– tumor uptake were low for nontargeted IgG<sub>1</sub> (generally < 1), indicating a lack of specific uptake.

**Pharmacokinetic Analysis.** To evaluate the blood pharmacokinetics of  $^{125}\text{I}$ -MORAb-004 in naïve versus TEM1+ tumor-bearing *nu/nu*

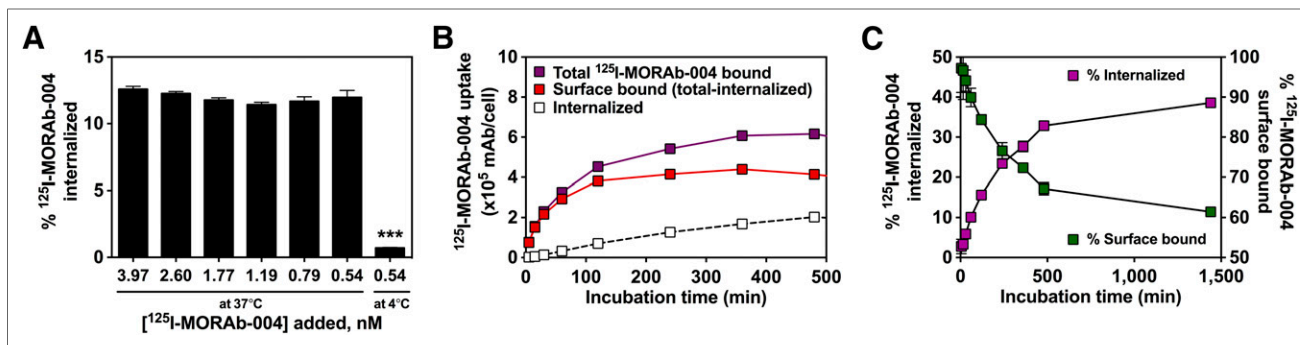


**FIGURE 3.** Internalization of  $^{125}\text{I}$ -MORAb-004 by MS1-TEM1/fLuc cells with respect to total amount of mAb bound per cell after incubation at 37°C as function of dose (A) and time (B–C). Internalization was measured in presence or absence of excess of unlabeled MORAb-004 (100 nM) in incubation medium to block hTEM1 surface protein binding. (C) Internalized fraction of  $^{125}\text{I}$ -MORAb-004 over time as function of total cell-associated radioactivity. Values shown are mean of 3 independent experiments performed in quadruplicate. \*\*\* $P$  value < 0.001.

mice, serum samples were collected and analyzed at defined times (supplemental material). Blood-pool clearance rates were slow for the targeted IgG<sub>1</sub> mAb in naïve mice as compared with mice with TEM1+ tumors: the fast  $\alpha$ -phase of the biphasic blood clearance was 1.9 versus 1.1 h, respectively, whereas the slower  $\beta$ -phase was 117.9 h in naïve mice, compared with 28.8 h in tumor-bearing mice ( $R^2 = 0.95$  and 0.92, respectively). For further comparison, the  $\alpha$ - and  $\beta$ -decay rates for blood clearance of the isotype control  $^{125}\text{I}$ -IgG<sub>1</sub> in tumor-bearing mice were 3.7 and 76.9 h, respectively. These rates were both slower than those for  $^{125}\text{I}$ -MORAb-004 in tumor-bearing mice, further demonstrating targeting specificity of  $^{125}\text{I}$ -MORAb-004 for TEM1+ tumors.

**PET Imaging Studies.** Tumor location and volume were first confirmed by in vivo bioluminescence imaging of fLuc reporter gene expression in mice bearing subcutaneous ID8 tumor grafts with MS1-TEM1-expressing vasculature on the left flank and control MS1/ID8 tumor graft on the right flank.  $^{124}\text{I}$ -MORAb-004 uptake in tumor grafts was TEM1-specific, as demonstrated by target-blocking experiments performed by coinjecting an excess dose (25  $\mu\text{g}$ ) of nonlabeled cold MORAb-004 (Fig. 5B). TEM1+ tumors were poorly visualized throughout the 3-d study period, demonstrating TEM1 specificity of MORAb-004. Images for the remaining mice in the PET study are provided in the supplemental materials. Postmortem tissue sampling of the mice after 72-h PET imaging confirmed the biodistribution data. The tumor uptake of  $^{124}\text{I}$ -MORAb-004 was  $221.82 \pm 57.33$  %ID/g in TEM1+ tumor grafts at 72 h after injection and was significantly greater than corresponding tumor uptake of  $24.06 \pm 3.26$  %ID/g at 72 h in mice blocked with excess cold MORAb-004, again confirming radioimmunoconjugate specificity (supplemental material). In contrast, no significant difference in tumor uptake was observed in TEM1 tumor grafts after coinjection with blocking dose of MORAb-004 (Fig. 5B).

## DISCUSSION

The tumor vascular marker TEM1/endothelial is emerging as an attractive biomarker for targeted molecular diagnostics and therapeutics because of its expression across many human tumors, low to absent expression in normal tissues, and accessibility from the vascular circulation. Although the molecular function of TEM1 remains unclear, investigators have recently designed IgG antibodies targeting the lectin-like domain of TEM1, which inhibit cell migration (20) and vascular tube formation (9,32,33). Smaller

scFv constructs have also been reported for TEM1 targeting of drug-delivery vehicles (19) or diagnostics for fluorescence imaging techniques (17). Although TEM1 is a quasiuniversal tumor target present in the vasculature of many solid tumor types, a variable proportion of tumors—depending on histotype—show low or no TEM1 expression (6). Detection of TEM1 in tumors may facilitate the selection of patients for specific therapies and would allow monitoring of therapeutic effect in real time using immuno-PET (25,34,35). Combined with the ready availability of  $^{124}\text{I}$  and its sufficiently long half-life (4.2 d),  $^{124}\text{I}$  immuno-PET imaging is an attractive approach to demonstrate quantitative biomarker expression noninvasively. In this work, we describe the detailed preclinical characterization of a novel PET radioimmundiagnostic humanized anti-TEM1  $^{124}\text{I}$ -MORAb-004 IgG<sub>1</sub>, of which the naked antibody MORAb-004 is currently in trials for cancer immunotherapy.

Direct radioiodination of MORAb-004 did not dramatically alter the functional targeting to MS1 mouse endothelial cells engineered to express recombinant hTEM1 (MS1-TEM1). This is evidenced by the nanomolar affinity, high cellular binding capacity (>10<sup>5</sup> antibodies bound per cell), and immunoreactivity of  $^{125}\text{I}/^{124}\text{I}$ -MORAb-004. Differences in degree and quality of hTEM1 glycosylation patterns in murine and human cells could potentially overestimate MORAb-004 accessibility and binding to native hTEM1. However, the affinity of  $^{125}\text{I}$ -MORAb-004 for native hTEM1 expressed in human neuroblastoma cancer cells is considerably higher than recombinant hTEM1 in murine endothelial cells, suggesting that MORAb-004 accessibility and affinity is sufficiently high for targeting to endogenous hTEM1 in patients. Antibody internalization and intracellular retention are important criteria for assessing the potential of a therapeutic agent being considered for conjugation with a toxin or radioisotope. Fluorescence microscopy of dye-labeled MORAb-004 and radiotracing of  $^{125}\text{I}$ -MORAb-004 confirm slow internalization (and radiolabel catabolism ex post facto) in vitro by MS1-TEM1 endothelial cells. Internalization was found to be even slower in human neuroblastoma cells endogenously expressing hTEM1. However, in vitro results may not always be indicative of antibody processing in vivo.

MORAb-004 binds to hTEM1 and does not cross-react with murine TEM1. Hence, we used a chimeric ovarian cancer vascular murine model recently described to assess the targeting of MORAb-004 to hTEM1 TVM (18). In this preclinical model, tumors derived from ID8 ovarian cancer cells enriched with MS1

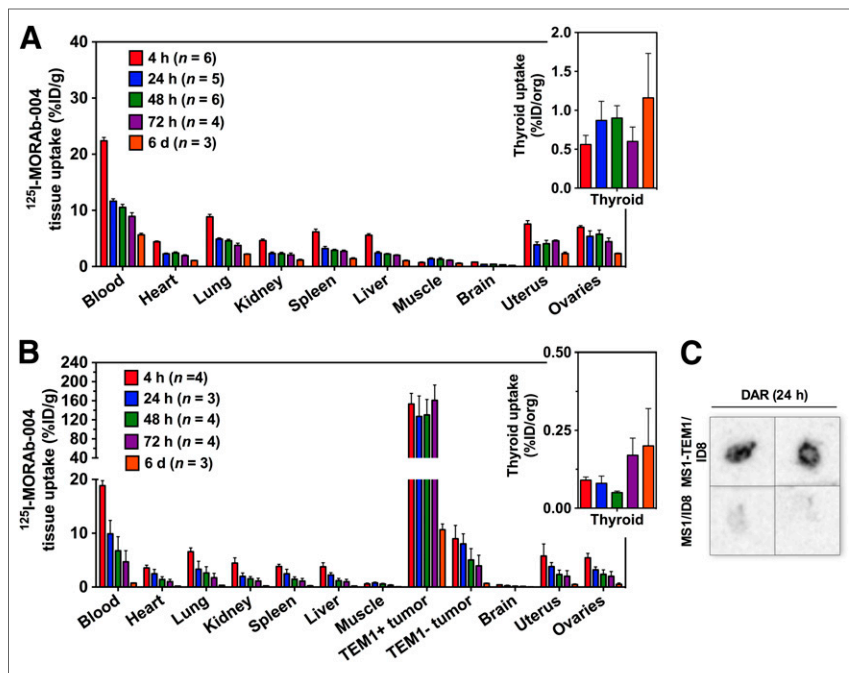


**FIGURE 4.** Biodistribution (%ID/g) of  $^{125}\text{I}$ -MORAb-004 (2.5  $\mu\text{g}/\text{mouse}$ ) in naive *nu/nu* female mice (A) and MS1-TEM1/ID8 and MS1/ID8 tumor-bearing mice (B). Insets are respective uptake of radioiodine in thyroid represented as %ID/org. Data are shown as mean  $\pm$  SD. There was significant difference between uptake in TEM1+ tumors as compared with TEM1- tumors.  $P < 0.001$ . (C) Digital autoradiography (DAR) of representative MS1-TEM1/ID8 and control MS1/ID8 tumors showing specific uptake of  $^{125}\text{I}$ -MORAb-004 24 h after injection in TEM1+ tumors only.

endothelial cells had increased vascular density, compared with ID8 tumors alone by visual inspection and from quantification of hemoglobin content (data not shown). This increase implies that MS1 cells contribute to the formation of functional tumor vasculature. Further, MS1-TEM1 cells admixed with ID8 cells integrate into the tumor vasculature, as confirmed by immunohistochemical visualization of hTEM1-positive vessels and capillaries (Supplemental Fig. 8).

Biodistribution data with this vascular hTEM1 murine model revealed high uptake of  $^{125}\text{I}$ -MORAb-004 ( $>150$  %ID/g at 4 h) in ID8 ovarian tumors with TEM1+ tumor vasculature and no up-

take in the contralateral hTEM1- ID8/MS1 tumors. This high degree of targeting to TEM1+ vessels was maintained up to 72 h after injection, with target tumor uptake decreasing on day 6. There was a low extent of thyroid uptake over the course of the biodistribution and PET study ( $<2$  %ID/org). This is consistent with previously reported studies with other radioiodine-labeled mAbs targeting slowly internalizing cell surface markers—including  $^{124}\text{I}$ -cG250 IgG mAb for imaging carbonic anhydrase 9 (CAIX) expression (25) and  $^{125}\text{I}$ -35A7 IgG mAb, as a radioimmunotherapeutic targeted to carcinoembryonic antigen (CEA) (36). Therefore, we can tentatively conclude that the antibody catabolic rate in vivo is comparable to that seen in vitro. It is plausible that slow intratumoral metabolism and subsequent recirculation of  $^{124}\text{I}$ -labeled metabolites may also occur. Full metabolic studies are beyond the scope of the current study and will be the subject of further investigations.

This type of preclinical model is a helpful tool for validating agents specific to human tumor vascular targets in the absence of more relevant knock-in models with the human coding sequence inserted into the mouse locus. Immuno-PET data demonstrate that  $^{124}\text{I}$ -MORAb-004 imaging provides high tumor-to-background tissue ratios and that this high uptake is specific for TEM1 expression in tumor tissue. On the basis of the aforementioned in vivo results,  $^{124}\text{I}$ -MORAb-004 has favorable pharmacokinetics, with rapid tumor targeting, rapid blood clearance, and fast washout from nontarget tissue. An experimental limitation to our preclinical model is that hTEM1 is exclusively expressed on engineered murine endothelial cells that integrate into the murine tumor vasculature, and so we are only able to assess targeting and tumor retention of MORAb-004 to the most easily accessible tumor vascular compartment. In human tumors, TEM1 is expressed by tumor-associated stromal cells, fibro-

ing provides high tumor-to-background tissue ratios and that this high uptake is specific for TEM1 expression in tumor tissue. On the basis of the aforementioned in vivo results,  $^{124}\text{I}$ -MORAb-004 has favorable pharmacokinetics, with rapid tumor targeting, rapid blood clearance, and fast washout from nontarget tissue. An experimental limitation to our preclinical model is that hTEM1 is exclusively expressed on engineered murine endothelial cells that integrate into the murine tumor vasculature, and so we are only able to assess targeting and tumor retention of MORAb-004 to the most easily accessible tumor vascular compartment. In human tumors, TEM1 is expressed by tumor-associated stromal cells, fibro-

**TABLE 2**  
Biodistribution of  $^{125}\text{I}$ -MORAb-004 in Naive Mice at Various Times After Injection\*

Organ	4 h (n = 6)	24 h (n = 5)	48 h (n = 6)	72 h (n = 4)	6 d (n = 4)
Blood	22.39 $\pm$ 1.47	11.64 $\pm$ 0.95	10.53 $\pm$ 1.32	8.93 $\pm$ 1.30	5.64 $\pm$ 0.50
Heart	4.40 $\pm$ 0.38	2.26 $\pm$ 0.32	2.40 $\pm$ 0.52	1.94 $\pm$ 0.30	1.06 $\pm$ 0.10
Lungs	8.85 $\pm$ 1.06	4.88 $\pm$ 0.47	4.58 $\pm$ 0.66	3.76 $\pm$ 0.80	2.20 $\pm$ 0.15
Kidney	4.61 $\pm$ 0.69	2.32 $\pm$ 0.57	2.28 $\pm$ 0.62	2.06 $\pm$ 0.69	1.14 $\pm$ 0.27
Spleen	6.17 $\pm$ 1.20	3.20 $\pm$ 0.84	2.88 $\pm$ 0.46	2.71 $\pm$ 0.42	1.40 $\pm$ 0.29
Liver	5.56 $\pm$ 0.71	2.41 $\pm$ 0.57	2.21 $\pm$ 0.31	2.00 $\pm$ 0.22	1.03 $\pm$ 0.22
Muscle	0.69 $\pm$ 0.31	1.36 $\pm$ 0.44	1.28 $\pm$ 0.69	1.11 $\pm$ 0.18	0.55 $\pm$ 0.18
Brain	0.77 $\pm$ 0.11	0.37 $\pm$ 0.08	0.40 $\pm$ 0.09	0.29 $\pm$ 0.09	0.18 $\pm$ 0.01
Uterus	7.55 $\pm$ 1.54	3.86 $\pm$ 1.16	4.06 $\pm$ 1.49	4.57 $\pm$ 0.31	2.30 $\pm$ 0.47
Ovaries	6.98 $\pm$ 0.75	5.36 $\pm$ 2.18	5.75 $\pm$ 1.81	4.42 $\pm$ 1.31	2.30 $\pm$ 0.18
Thyroid†	0.56 $\pm$ 0.29	0.87 $\pm$ 0.55	0.90 $\pm$ 0.39	0.60 $\pm$ 0.37	1.16 $\pm$ 0.99

\*Data are expressed as %ID/g  $\pm$  SD; mice injected with 0.185 MBq (5  $\mu\text{Ci}$ ); 2.5  $\mu\text{g}$  of IgG.

†Data are expressed as %ID/org  $\pm$  SD.

**TABLE 3**  
Biodistribution of  $^{125}\text{I}$ -MORAb-004 in Tumor-Bearing Mice at Various Times After Injection\*

Organ	4 h (n = 3)	24 h (n = 3)	48 h (n = 4)	72 h (n = 4)	6 d (n = 3)
Blood	18.84 ± 0.93	9.90 ± 2.49	6.75 ± 2.61	4.68 ± 2.09	0.74 ± 0.05
Heart	3.55 ± 0.51	2.48 ± 0.81	1.40 ± 0.53	1.00 ± 0.44	0.18 ± 0.04
Lungs	6.57 ± 0.71	3.32 ± 1.48	2.62 ± 1.16	1.75 ± 0.82	0.33 ± 0.02
Kidney	4.46 ± 0.98	1.98 ± 0.64	1.54 ± 0.41	1.13 ± 0.52	0.21 ± 0.04
Spleen	3.81 ± 0.43	2.47 ± 0.83	1.45 ± 0.46	1.10 ± 0.49	0.23 ± 0.08
Liver	3.76 ± 0.76	2.23 ± 0.43	1.19 ± 0.42	0.99 ± 0.45	0.19 ± 0.02
Muscle	0.58 ± 0.16	0.77 ± 0.15	0.58 ± 0.13	0.47 ± 0.29	0.06 ± 0.01
Brain	0.40 ± 0.06	0.25 ± 0.11	0.15 ± 0.07	0.12 ± 0.05	0.03 ± 0.01
Uterus	5.77 ± 2.25	3.79 ± 0.76	2.33 ± 0.82	2.00 ± 1.04	0.47 ± 0.12
Ovaries	5.44 ± 0.82	3.20 ± 0.56	2.37 ± 0.85	2.01 ± 0.87	0.51 ± 0.24
Thyroid†	0.09 ± 0.02	0.08 ± 0.04	0.05 ± 0.01	0.17 ± 0.11	0.20 ± 0.17
Tumors					
MS1-TEM1/ID8	153.19 ± 22.25	127.13 ± 42.87	130.27 ± 32.38	160.91 ± 32.09	10.65 ± 1.08
MS1/ID8	8.98 ± 2.48	8.03 ± 1.86	5.04 ± 2.12	3.93 ± 1.98	0.67 ± 0.08
Ratio of TEM1+ tumor to					
Blood	8.14 ± 1.13	12.36 ± 4.72	21.76 ± 9.15	40.64 ± 19.40	16.50 ± 3.68
Muscle	266.03 ± 84.62	164.35 ± 64.30	224.86 ± 74.10	340.03 ± 216.28	177.50 ± 34.63
TEM1- tumor	18.06 ± 5.10	16.51 ± 6.21	29.71 ± 13.29	49.14 ± 22.54	16.02 ± 2.51

\*Data are expressed as %ID/g ± SD; mice injected with 0.185 MBq [5  $\mu\text{Ci}$ ]; 2.5  $\mu\text{g}$  of IgG.

†Data are expressed as %ID/org ± SD.

blasts, and pericytes (7,24,37); various types of cancer cells; and endothelial progenitor cells (6,33). However, IgG can readily cross the leaky basement membrane of tumor vasculature and extravasate into the perivascular space, suggesting that MORAb-004 could bind readily to various cell types presenting surface TEM1 in the tumor microenvironment. Although this model cannot address questions including the temporal regulation of hTEM1 with respect to tumor size or on internalization of the antibody, the recent development of hTEM1 knock-in mice (38) will allow future studies to focus toward that goal.

Overall, the novel radiotracer  $^{124}\text{I}$ -MORAb-004 represents a promising candidate for further evaluation and translation to the clinic as an immuno-PET agent for the noninvasive detection of primary and metastatic cancers expressing TEM1 in vivo.

## CONCLUSION

The humanized anti-hTEM1 IgG mAb  $^{125}/^{124}\text{I}$ -MORAb-004 can be prepared by direct radioiodination, with high radiochemical purity and specific activity, without significant loss of specificity and immunoreactivity to hTEM1-positive cells. In vitro internalization is fairly low and protracted. Biodistribution and  $^{124}\text{I}$  immuno-PET in a chimeric hTEM1 mouse tumor model revealed robust TEM1-specific contrast within the tumor vasculature as early as 4 h and up to 6 d after administration. Autoradiography further confirmed microdistribution of  $^{124}\text{I}$ -MORAb-004 within TEM1-positive vascularized tumor tissue. This is the first report, to our knowledge, fully characterizing  $^{124}\text{I}$ -MORAb-004 as an immuno-PET diagnostic of noninvasive detection of hTEM1 in a murine tumor vascular network.

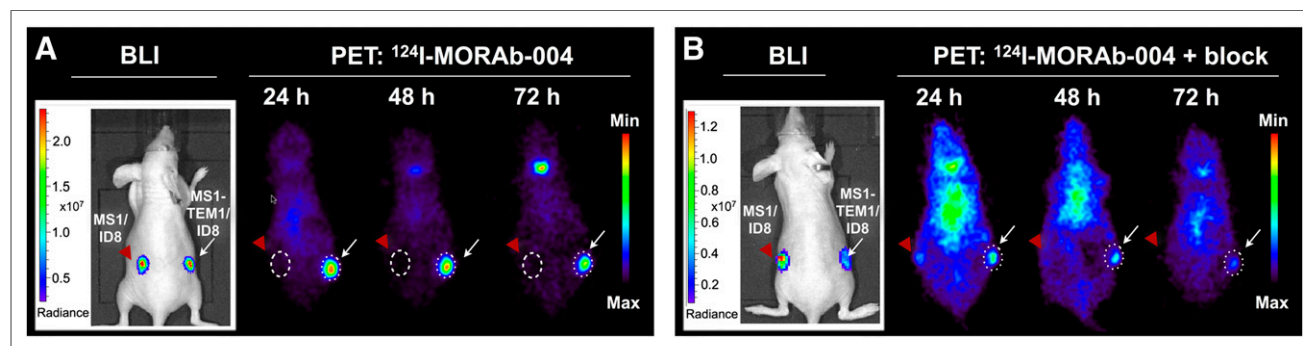


**FIGURE 5.** Longitudinal in vivo immuno-PET imaging of distribution of  $^{124}\text{I}$ -MORAb-004 in nude mice bearing subcutaneous chimeric ID8 tumor grafts over time. Mice were injected with  $^{124}\text{I}$ -MORAb-004 (5.2 MBq, 2.5  $\mu\text{g}$  mAb) (A) or co-injected with 25  $\mu\text{g}$  of unlabeled MORAb-004 (B) and scanned for 1 h at different time points after injection. Transverse projections of 1 mouse from each group are shown, with representative images of photon radiance from bioluminescence imaging of tumor grafts enriched with luciferase (fLuc)-transfected MS1 or MS1-TEM1 endothelial cells of respective mouse shown to left of each PET panel. (A) Increased uptake of  $^{124}\text{I}$ -MORAb-004 was observed in tumors expressing TEM1+ tumor (right, white arrow), compared with control tumor (left, red arrowhead). (B) Specific blocking of  $^{124}\text{I}$ -MORAb-004 uptake in TEM1+ tumor observed after administration of excess unlabeled mAb. BLI = bioluminescence imaging.

## DISCLOSURE

The costs of publication of this article were defrayed in part by the payment of page charges. Therefore, and solely to indicate this fact, this article is hereby marked "advertisement" in accordance with 18 USC section 1734. This work was supported by NIH Transformative R01CA156695 and NIH NCCR and NCATS, through grant KL2TR00139; the Honorable Tina Brozman Foundation; and a grant from the Bassler Center at the University of Pennsylvania. No other potential conflict of interest relevant to this article was reported.

## ACKNOWLEDGMENTS

We thank Eric Blankemeyer of the University of Pennsylvania Small Animal Imaging Facility (SAIF) for excellent technical support.

## REFERENCES

1. St. Croix B, Rago C, Velculescu V, et al. Genes expressed in human tumor endothelium. *Science*. 2000;289:1197–1202.
2. Carson-Walter EB, Watkins DN, Nanda A, Vogelstein B, Kinzler KW, St. Croix B. Cell surface tumor endothelial markers are conserved in mice and humans. *Cancer Res*. 2001;61:6649–6655.
3. Buckanovich RJ, Sasaroli D, O'Brien-Jenkins A, et al. Tumor vascular proteins as biomarkers in ovarian cancer. *J Clin Oncol*. 2007;25:852–861.
4. Rettig WJ, Garin-Chesa P, Healey JH, Su SL, Jaffe EA, Old LJ. Identification of endosialin, a cell surface glycoprotein of vascular endothelial cells in human cancer. *Proc Natl Acad Sci USA*. 1992;89:10832–10836.
5. Christian S, Ahorn H, Koehler A, et al. Molecular cloning and characterization of endosialin, a C-type lectin-like cell surface receptor of tumor endothelium. *J Biol Chem*. 2001;276:7408–7414.
6. Rouleau C, Curiel M, Weber W, et al. Endosialin protein expression and therapeutic target potential in human solid tumors: sarcoma versus carcinoma. *Clin Cancer Res*. 2008;14:7223–7236.
7. Simonavicius N, Robertson D, Bax DA, Jones C, Huijbers IJ, Isacke CM. Endosialin (CD248) is a marker of tumor-associated pericytes in high-grade glioma. *Mod Pathol*. 2008;21:308–315.
8. Christian S, Winkler R, Helfrich I, et al. Endosialin (Tem1) is a marker of tumor-associated myofibroblasts and tumor vessel-associated mural cells. *Am J Pathol*. 2008;172:486–494.
9. Bagley RG. Endosialin: from vascular target to biomarker for human sarcomas. *Biomark Med*. 2009;3:589–604.
10. Davies G, Cunnick GH, Mansel RE, Mason MD, Jiang WG. Levels of expression of endothelial markers specific to tumour-associated endothelial cells and their correlation with prognosis in patients with breast cancer. *Clin Exp Metastasis*. 2004;21:31–37.
11. Teicher BA. Newer vascular targets: endosialin. *Int J Oncol*. 2007;30:305–312.
12. Valdez Y, Maia M, Conway EM. CD248: reviewing its role in health and disease. *Curr Drug Targets*. 2012;13:432–439.
13. Carson-Walter EB, Winans BN, Whiteman MC, et al. Characterization of TEM1/endosialin in human and murine brain tumors. *BMC Cancer*. 2009;9:417.
14. Rmali KA, Puntis MC, Jiang WG. Prognostic values of tumor endothelial markers in patients with colorectal cancer. *World J Gastroenterol*. 2005;11:1283–1286.
15. Dolznig H, Schweifer N, Puri C, et al. Characterization of cancer stroma markers: in silico analysis of an mRNA expression database for fibroblast activation protein and endosialin. *Cancer Immun*. 2005;5:10.
16. Opavsky R, Haviernik P, Jurkovicova D, et al. Molecular characterization of the mouse Tem1/endosialin gene regulated by cell density in vitro and expressed in normal tissues in vivo. *J Biol Chem*. 2001;276:38795–38807.
17. Zhao A, Nunez-Cruz S, Li C, Coukos G, Siegel DL, Scholler N. Rapid isolation of high-affinity human antibodies against the tumor vascular marker Endosialin/TEM1, using a paired yeast-display/secretory scFv library platform. *J Immunol Methods*. 2011;363:221–232.
18. Li C, Swails JL, Hasegawa K, et al. In vivo modeling and detection of the ovarian cancer vascular marker TEM1. Paper presented at: American Association for Cancer Research (AACR)—Third International Conference on Molecular Diagnostics in Cancer Therapeutic Development; September 22–25, 2008; Philadelphia, PA, United States.
19. Marty C, Langer-Machova Z, Sigrist S, Schott H, Schwendener RA, Ballmer-Hofer K. Isolation and characterization of a scFv antibody specific for tumor endothelial marker 1 (TEM1), a new reagent for targeted tumor therapy. *Cancer Lett*. 2006;235:298–308.
20. Tomkowicz B, Rybinski K, Foley B, et al. Interaction of endosialin/TEM1 with extracellular matrix proteins mediates cell adhesion and migration. *Proc Natl Acad Sci USA*. 2007;104:17965–17970.
21. Sarcoma Study of MORAb-004 Utilization: Research and Clinical Evaluation. (SOURCE). ClinicalTrials.gov. March 5, 2013. <http://clinicaltrials.gov/show/NCT01574716>. Accessed January 16, 2014.
22. Becker R, Lenter MC, Vollkommer T, et al. Tumor stroma marker endosialin (Tem1) is a binding partner of metastasis-related protein Mac-2 BP90K. *FASEB J*. 2008;22:3059–3067.
23. Brady J, Neal J, Sadakar N, Gasque P. Human endosialin (tumor endothelial marker 1) is abundantly expressed in highly malignant and invasive brain tumors. *J Neuropathol Exp Neurol*. 2004;63:1274–1283.
24. MacFadyen JR, Haworth O, Roberson D, et al. Endosialin (TEM1, CD248) is a marker of stromal fibroblasts and is not selectively expressed on tumour endothelium. *FEBS Lett*. 2005;579:2569–2575.
25. Divgi CR, Pandit-Taskar N, Jungbluth AA, et al. Preoperative characterisation of clear-cell renal carcinoma using iodine-124-labelled antibody chimeric G250 (<sup>124</sup>I-cG250) and PET in patients with renal masses: a phase I trial. *Lancet Oncol*. 2007;8:304–310.
26. Kenanova V, Olafsen T, Crow DM, et al. Tailoring the pharmacokinetics and positron emission tomography imaging properties of anti-carcinoembryonic antigen single-chain Fv-Fc antibody fragments. *Cancer Res*. 2005;65:622–631.
27. Sundaresan G, Yazaki PJ, Shively JE, et al. <sup>124</sup>I-labeled engineered anti-CEA minibodies and diabodies allow high-contrast, antigen-specific small-animal PET imaging of xenografts in athymic mice. *J Nucl Med*. 2003;44:1962–1969.
28. Williams SR, Son DS, Terranova PF. Protein kinase C delta is activated in mouse ovarian surface epithelial cancer cells by 2,3,7,8-tetrachlorodibenzo-p-dioxin (TCDD). *Toxicology*. 2004;195:1–17.
29. Bailey G. The Iodogen method for radiolabeling protein. In: Walker JM, ed. *The Protein Protocols Handbook*. Totowa, NJ: Humana Press, Inc.; 1996:673–674.
30. Chacko AM, Nayak M, Greineder CF, Delisser HM, Muzykantov VR. Collaborative enhancement of antibody binding to distinct PECAM-1 epitopes modulates endothelial targeting. *PLoS ONE*. 2012;7:e34958.
31. Surti S, Karp JS, Perkins AE, et al. Imaging performance of A-PET: a small animal PET camera. *IEEE Trans Med Imaging*. 2005;24:844–852.
32. Bagley RG, Honma N, Weber W, et al. Endosialin/TEM 1/CD248 is a pericyte marker of embryonic and tumor neovascularization. *Microvasc Res*. 2008;76:180–188.
33. Bagley RG, Rouleau C, St Martin T, et al. Human endothelial precursor cells express tumor endothelial marker 1/endosialin/CD248. *Mol Cancer Ther*. 2008;7:2536–2546.
34. Pryma DA, O'Donoghue JA, Humm JL, et al. Correlation of in vivo and in vitro measures of carbonic anhydrase IX antigen expression in renal masses using antibody <sup>124</sup>I-cG250. *J Nucl Med*. 2011;52:535–540.
35. O'Donoghue JA, Smith-Jones PM, Humm JL, et al. <sup>124</sup>I-huA33 antibody uptake is driven by A33 antigen concentration in tissues from colorectal cancer patients imaged by immuno-PET. *J Nucl Med*. 2011;52:1878–1885.
36. Santoro L, Boutaleb S, Garambois V, et al. Noninternalizing monoclonal antibodies are suitable candidates for <sup>125</sup>I radioimmunotherapy of small-volume peritoneal carcinomatosis. *J Nucl Med*. 2009;50:2033–2041.
37. Wesseling P, Schlingemann RO, Rietveld FJ, Link M, Burger PC, Ruiter DJ. Early and extensive contribution of pericytes/vascular smooth muscle cells to microvascular proliferation in glioblastoma multiforme: an immuno-light and immuno-electron microscopic study. *J Neuropathol Exp Neurol*. 1995;54:304–310.
38. Krauthauser C, Grasso L, Nicolaidis NC, Lin JM. Neutralizing Endosialin antibody, MORAb-004, enhances efficacy of TAXOTERE in a metastatic melanoma model. *Cancer Res*. 2012;72(suppl 1):4410.